Fragment-Based Discovery of the Pyrazol-4-yl Urea (AT9283), a Multitargeted Kinase Inhibitor with Potent Aurora Kinase Activity†

Steven Howard,* Valerio Berdini, John A. Boulstridge, Maria G. Carr, David M. Cross, Jayne Curry, Lindsay A. Devine, Theresa R. Early, Lynsey Fazal, Adrian L. Gill, Michelle Heathcote, Sarita Maman, Julia E. Matthews, Rachel L. McMenamin, Eva F. Navarro, Michael A. O'Brien, Marc O'Reilly, David C. Rees, Matthias Reule, Dominic Tisi, Glyn Williams, Mladen Vinković, and Paul G. Wyatt

Astex Therapeutics Ltd., 436 Cambridge Science Park, Milton Road, Cambridge, CB4 0QA, U.K.

Received August 4, 2008

Here, we describe the identification of a clinical candidate via structure-based optimization of a ligand efficient pyrazole-benzimidazole fragment. Aurora kinases play a key role in the regulation of mitosis and in recent years have become attractive targets for the treatment of cancer. X-ray crystallographic structures were generated using a novel soakable form of Aurora A and were used to drive the optimization toward potent ($IC_{50} \approx 3$ nM) dual Aurora A/Aurora B inhibitors. These compounds inhibited growth and survival of HCT116 cells and produced the polyploid cellular phenotype typically associated with Aurora B kinase inhibition. Optimization of cellular activity and physicochemical properties ultimately led to the identification of compound **16** (AT9283). In addition to Aurora A and Aurora B, compound **16** was also found to inhibit a number of other kinases including JAK2 and Abl (T315I). This compound demonstrated in vivo efficacy in mouse xenograft models and is currently under evaluation in phase I clinical trials.

Introduction

Fragment-based drug discovery is a rapidly growing technique in medicinal chemistry that differs from more traditional approaches based on chemical leads derived from high throughput screening. The field has been reviewed extensively over recent years.[1−6] Fragments are low molecular weight compounds (typically 100−250 Da) with generally low binding affinities that, as a result, typically require very sensitive biophysical screening methods such as X-ray crystallography,[7,8] nuclear magnetic resonance spectroscopy (NMR),[9] and surface plasmon resonance (SPR).[10] An advantage of starting with fragments is that despite their often low affinity, fragments generally possess good ligand efficiency (LE[a])[11,12]and as such form a small number of very high quality binding interactions with their protein target. LE is the ratio of free binding affinity to molecular size. It is possible to optimize fragments to relatively low molecular weight leads, and this can be achieved with a limited number of molecules, particularly if good structural data are available. Fragment-based drug discovery has been used in several laboratories to generate leads that have been progressed into clinical trials.[6] From our own laboratories fragment screening and subsequent structure-based drug design have led to three compounds currently in clinical trials in cancer patients, including a CDK inhibitor,[13] an HSP90 inhibitor, and the Aurora kinase inhibitor **16** described herein.

The Aurora enzymes are serine/threonine kinases that are known to be important regulators of mitosis.[14] In recent years, two isoforms, Aurora A and Aurora B, have been of considerable interest as targets in the discovery of new anticancer drugs.[15] This interest stems from the fact that both isoforms are found overexpressed in solid tumors and leukemias.[16−19] Moreover, experimental data suggest that inappropriately high levels of Aurora kinase activity are linked to genetic instability and cancer.[20]

Small molecule leads for Aurora kinases have been identified from both high throughput screening and, more recently, from fragment-based approaches.[21−23] In the latter case, Erlanson et al. employed a fragment-based DCC (dynamic combinatorial chemistry) strategy while Warner and Hurley used computational docking in combination with a structural model of Aurora A in order to identify fragments. The effect of small molecule Aurora kinase inhibitors on cells has been well described in the literature.[24−28] Typically, dual Aurora A/Aurora B inhibitors result in cellular phenotypes predominantly related to Aurora B inhibition. This is characterized by rapid inhibition of serine-10 phosphorylation on histone H3 and aberrant mitosis leading to failed cytokinesis and endoreduplication. Cells adopt a polyploid morphology and ultimately undergo apoptosis. To date, several potent inhibitors of Aurora kinases such as **1** (VX-680/MK-0457) and **2** (PHA739358) have been progressed into clinical trials (Figure 1).[26,29−31] Interestingly, in addition to inhibition of both Aurora A and Aurora B isoforms, these compounds also inhibit a number of other kinases including Flt-3 and Abl (compound **1**) and FGFR1, RET, and Abl (compound **2**), all of which have been suggested as targets for cancer drug discovery. More recently, isoform selective compounds have been described including **3** (AZD1152, Aurora B selective) and **4** (MLN8054, Aurora A selective).[32−34] However, it remains to be seen precisely what type of molecular profile will be most desirable in a safe and effective Aurora kinase inhibitor.

† Coordinates of the protein complexes with compounds **5**, **7**, **9**, **10**, and **16** have been deposited in the Protein Data Bank under accession codes 2w1d, 2w1f, 2w1c, 2w1e, 2w1g (Aurora A), 2w1h (CDK2), and 2w1i (JAK2).

* To whom correspondence should be addressed. Phone: +44 (0)1223 226209. Fax: +44 (0)1223 226201. E-mail: s.howard@astex-therapeutics.com.

[a] Abbreviations: CDK, cyclin dependent kinase; EDC, 1-(3-dimethyaminopropyl)-3-ethylcarbodiimide; LE, ligand efficiency ($LE = -\Delta G$ /HAC $\approx -RT \ln(IC_{50})$/HAC); HAC, heavy atom count; HBD, hydrogen bond donor; NOE, nuclear Overhauser effect; PPB, plasma protein binding; *T*/*C*, mean tumor volume of treated animals divided by the mean control tumor volume.

10.1021/jm800984v CCC: $40.75
Published on Web 12/30/2008

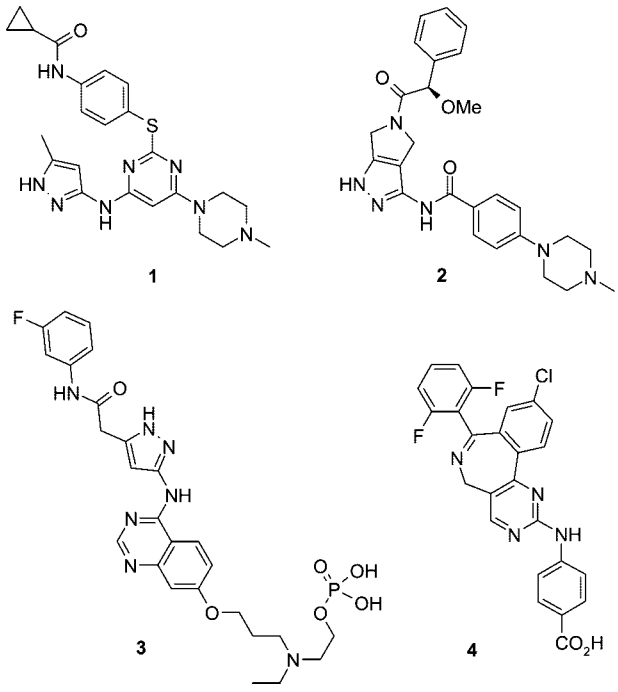

Figure 1

In this paper we describe the discovery of a multitargeted kinase inhibitor with potent Aurora kinase activity. Compounds were demonstrated to have potent cellular activity and to induce phenotypical changes that were consistent with Aurora kinase inhibition being the predominant effect.

Results and Discussion

Hit Generation. Pyrazole-benzimidazole fragment **5** was previously identified in our laboratories as a starting point for the development of CDK inhibitors (Scheme 1).[13] Subsequently a structure-based approach using CDK2 crystallography resulted in the identification of the benzamide analogue **7**. During the course of this work it was established that these pyrazole-benzimidazoles also had good activity and ligand efficiency for Aurora A. Moreover, fragment **5** demonstrated superior ligand efficiency (LE = 0.59) for Aurora A compared to CDK1 and CDK2 (Table 1). Unlike some fragment hits, **5** demonstrated sufficient potency to allow detection in a conventional enzyme bioassay.

Table 1. SAR for Amide Analogues

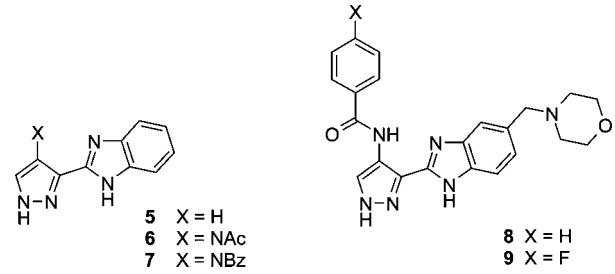

compd	IC$_{50}$ (μM)[a] Aurora A	LE[c]	Aurora B	CDK1/B	CDK2/A	HCT116 assay (μM)[b]
5	0.91	0.59	6.5	49% I @ 1000 μM	28	NT[e]
6	0.070	0.54	0.51	3.2	0.99	NT[e]
7	0.0059	0.49	0.18	0.23	0.052	3*
8	0.0035	0.38	0.015	0.34	0.14	0.1*
9	0.010	0.35	0.075	1.5	0.53	0.3
1[d]	0.0014	0.37	0.017	NT[e]	NT[e]	0.03*

[a] IC$_{50}$ values are given as the average of two or more determinations. [b] Primary cellular assay. HCT116 cells were incubated with test compound for 72 h and then examined for signs of polyploidy. The lowest concentration of compound required to produce a distinct polyploid phenotype was quoted (polyploidy is a direct result of Aurora B kinase inhibition). Compounds were tested in duplicate (unless otherwise indicated by an asterisk (*), where $n = 1$) and the results given as either a single number or a range. [c] LE = ligand efficiency with respect to Aurora A (LE = $-\Delta G$ /HAC $\approx -RT \ln(IC_{50})$/HAC). [d] Previously described Aurora kinase inhibitor **1**[26] [e] NT = not tested.

Compounds **5** and **7** were selected for further characterization with a view to optimization of their Aurora kinase activity. X-ray crystallographic structures for each compound were solved using a soakable crystal form of activated Aurora A.[35] In the case of fragment **5** the X-ray crystal structure showed the ligand sitting deeply in the ATP-binding site of Aurora A (Figure 2a). The ligand hydrogen-bonds to backbone carbonyl of Glu211 and also to the backbone NH and carbonyl of Ala213 of the protein hinge region. In Aurora A, the benzimidazole motif binds in the cleft defined by Ala213, Pro214, Leu215, and Gly216. This cleft has significant differences compared to the comparable region in CDK2 (defined by Leu83-Gln85). In particular, this region in Aurora A is largely defined by an extra glycine residue (Gly216) that is absent in CDK2. Consequently, the H-bond that exists in Aurora A between the carbonyl of Ala213 and

Scheme 1. Fragment Based Identification of Pyrazole-benzimidazole **7** Starting from Fragment **5**[a]

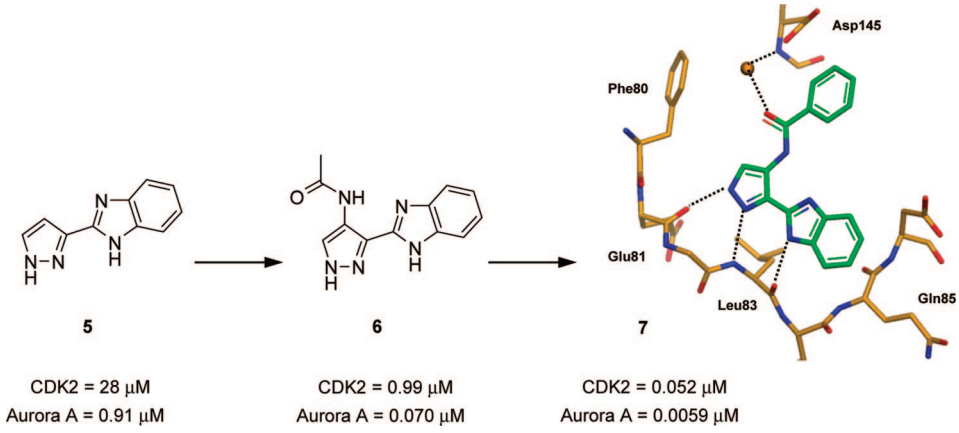

[a] Compounds were optimized for CDK2 by targeting the region around Asp145.[13] The crystal structure of **7** bound to CDK2 (ATP pocket) is shown with protein structure drawn in orange and key ligand−protein H-bonds indicated by the dotted lines.

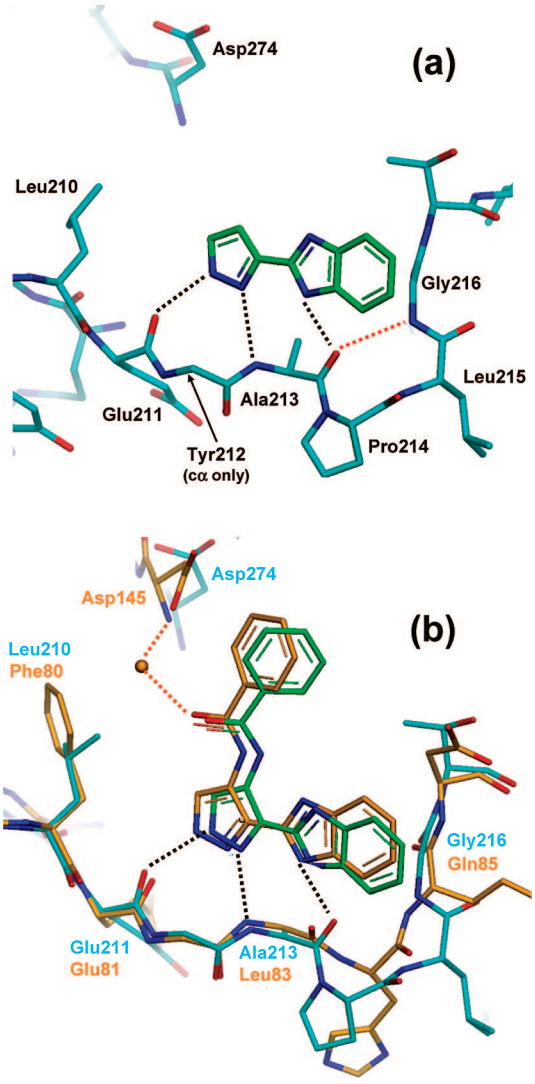

Figure 2. (a) Crystal structure of pyrazole-benzimidazole fragment **5** complexed with Aurora A, showing hydrogen bonding to the kinase hinge region (black lines) and hydrogen bonding between Ala213 and Gly216 (red line). Side chain of Tyr212 is omitted for clarity. (b) Overlay of the crystal structures of benzamide **7** bound to Aurora A (protein in blue, ligand in green, H-bonds as black dotted lines) and bound to CDK2 (protein and ligand in orange). Water mediated hydrogen bonds between **7** and Asp145 (CDK2) are shown by the orange dotted lines.

the NH of Gly216 has no counterpart in CDK2. This results in the cleft being more hydrophobic in nature, relative to CDK2, and leads to Aurora A having a higher affinity for flat aromatic fragments such as **5** (Aurora A $IC_{50} = 0.91\ \mu M$, CDK2 $IC_{50} = 28\ \mu M$). The structural rationale for the selectivity together with the good ligand efficiency of **5** led us to conclude that the pyrazole-benzimidazole core scaffold could be considered a good fragment starting point for the discovery of Aurora kinase inhibitors.

The binding mode of **7** showed the ligand making the same three hydrogen bonds to the hinge region (Figure 2b). An intramolecular H-bond exists between the benzimidazole and the amide NH, holding the molecule in a planar conformation. The region of the ATP pocket occupied by the benzamide motif also shows significant differences between Aurora A and CDK2. In the case of CDK2, the amide carbonyl of **7** makes a water mediated hydrogen bond to the backbone NH of Asp145 (CDK2). Furthermore, the benzene ring is in contact with the carboxylate side chain of this aspartate residue. Asp145 is part

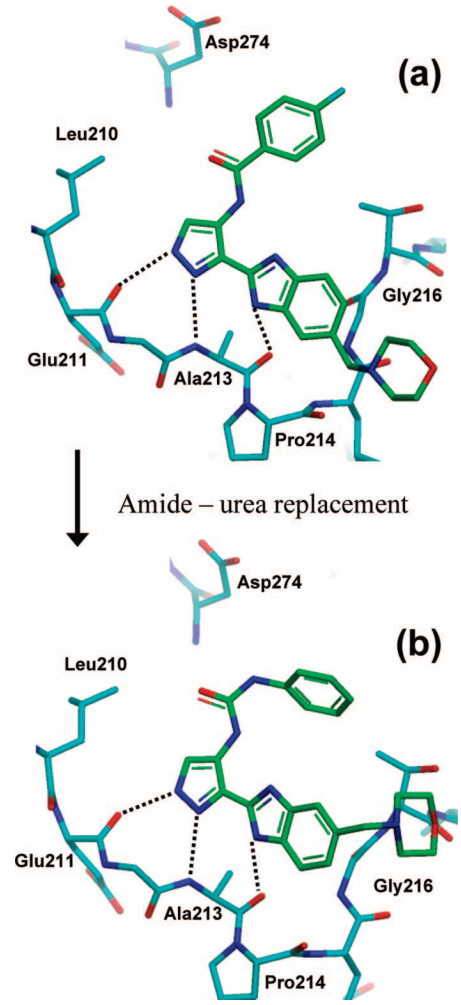

Figure 3. (a) Crystal structure of amide **9** complexed with Aurora A. (b) Crystal structure of **10** complexed with Aurora A showing the cis/trans configuration of the urea linker and partially twisted phenyl ring.

of the DFG motif that lies within the activation loop of serine and threonine kinases. Comparison of the Aurora A and CDK2 crystal structures revealed that the DFG motif adopts different conformations in the two proteins. In contrast to CDK2, the conformation of the DFG loop seen in Aurora A structures prohibits interaction between the ligand **7** and the corresponding residue Asp274.

Hit-to-Lead Phase. In contrast to the pyrazole-based CDK inhibitors described in our previous publication,[13] the aim of this work was to identify compounds that intervene in the cell-cycle process primarily via inhibition of Aurora kinases A and B. Although a measure of potency and selectivity for these enzyme targets was available from in vitro recombinant enzyme assays, a functional indication of selective Aurora B inhibition in cells was provided by the well described polyploid phenotype described in the Introduction. The optimization of the pyrazole-benzimidazole series focused on maximizing the in vitro potency for both Aurora A and Aurora B isoforms in addition to routinely screening for a polyploid phenotype in HCT116 cells.[36]

As a starting point for optimization, it was considered that the modest cellular potency of **7** (polyploidy observed at 3 μM) could be improved by introducing a basic motif. This strategy has been successful for other classes of kinase inhibitors.[13,37] An examination of the binding mode of **7** suggested that the 5- or 6-position of the benzimidazole could be further function-

Table 2. SAR of Urea Analogues

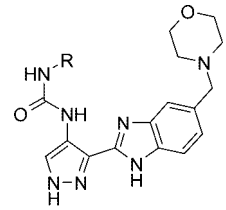

		IC$_{50}$ (μM)[a]						
compd	R	Aurora A	LE[c]	Aurora B	CDK1/B	CDK2/A	clogP	HCT116 assay (μM)[b]
10	phenyl	0.012	0.35	0.054	5.5	1.8	3.7	0.3−1
11	2-fluorophenyl	0.0028	0.36	0.010	1.1	0.23*	3.5	0.1−0.3
12	2,6-difluorophenyl	0.0015	0.36	0.0026	0.29	0.16	3.2	0.03
13	cyclohexyl	0.0057	0.36	0.0052	2.9	1.2	3.9	0.1
14	3-pyridinyl	0.013	0.35	0.024	0.29	0.16	2.6	1−3
15	4-tetahydropyranyl	0.026	0.33	0.010	17	NT[d]	1.5	1
16	cyclopropyl	52% I @ 3 nM	0.42	58% I @ 3 nM	1.7	0.51	2.2	0.03

[a] IC$_{50}$ values are given as the average of two or more determinations unless otherwise indicted by an asterisk (*) (where $n = 1$). [b] Primary cellular assay. HCT116 cells were incubated with test compound for 72 h and then examined for signs of polyploidy. The lowest concentration of compound required to produce a distinct polyploid phenotype was quoted (polyploidy is a direct result of Aurora B kinase inhibition). [c] LE = ligand efficiency with respect to Aurora A (LE = $-\Delta G$ /HAC $\approx -RT \ln(IC50)/HAC$). [d] NT = not tested.

alized without causing any clashes with the protein. Given that the series already possessed three hydrogen bond donors, a weakly basic morpholine group (p$K_a \approx 7$) was chosen in order minimize the increase in effective hydrogen bond donors. This initial strategy, as exemplified by **8** and **9**, was successful in increasing cellular potency (Table 1). The increase in cellular potency (comparing **8** with **7**) was most likely due to the associated 10-fold increase in affinity for Aurora B. Of these two compounds, the *p*-fluorophenyl analogue **9** was found to have encouraging pharmacokinetic properties in mouse (Clp = 43 (mL/min)/kg, $F_{po} = 26\%$), although plasma protein binding was found to be high (PPB = 99.5%). Subsequent optimization was therefore aimed at identifying compounds with reduced plasma protein binding and that maintained a similar in vitro profile to amides **8** and **9**.

Lead Optimization. A successful strategy to reduce plasma protein binding was conceived on the basis of making broad changes to the molecular pharmacophore. In support of this, the X-ray crystal structure of **9** complexed with Aurora A was solved in order to guide compound design (Figure 3a). Analysis of the structure revealed that the pyrazole-benzimidazole motif has excellent complementarity with the narrow region of the ATP pocket. This supported the decision to retain this motif in future designs as a key driver for potency and selectivity. Likewise, it was considered important to retain the 5-morpholinomethyl motif, as it had been shown to increase affinity for Aurora B. In contrast to the pyrazole-benzimidazole motif, the *p*-fluorophenyl group only partially fills the surrounding region of the ATP pocket and leaves a significant amount of space to accommodate molecules with modification in this region. Furthermore, the glycine loop is known to be flexible and therefore may tolerate significant modifications to the benzamide motif. Replacing the amide linker with a urea motif offered an opportunity to significantly modify the molecular shape without adding excessive molecular weight. This strategy was successful in significantly reducing plasma protein binding while maintaining a comparable in vitro profile as exemplified by urea **10** (mouse PPB = 95.3%) (Table 2). Analysis of the crystal structure of **10** complexed with Aurora A showed a similar binding mode to the hinge region of Aurora A kinase as seen with previous compounds (Figure 3b). The urea linker adopted a cis/trans configuration resulting in the molecule having a folded conformation with the phenyl ring placed in proximity to the benzimidazole. This binding mode necessitates the phenyl ring to adopt a partly twisted conformation relative to the plane of the pyrazole-benzimidazole scaffold.

Further optimization was aimed at improving the affinity for both Aurora kinases and increasing cellular potency. Considering the physicochemical properties of **10** (MW = 417, clogP = 3.7 and 4 HBD), care was taken to keep increases in clogP and MW to a minimum. Furthermore, an increase in the hydrogen bond donor (HBD) count was considered unacceptable in order to maintain cellular penetration.

An initial strategy to improve enzyme potency was aimed at reinforcing the twisted conformation of the phenyl ring by introducing *o*-fluoro substituents, e.g., **11** (Aurora A IC$_{50}$ = 2.8 nM) and **12** (Aurora A IC$_{50}$ = 1.5 nM) (Table 2). This correlated with improved activity in the HCT116 cellular assay (polypolidy observed as 0.1−0.3 and 0.03 μM, respectively). An alternative strategy replaced the phenyl ring with a saturated cyclohexyl group as exemplified by **13**. As with the *o*-fluorophenyl urea **11**, the cyclohexyl group would be expected to adopt a conformation with the plane of the ring being twisted relative to the pyrazole-benzimidazole scaffold. Compared to **10**, compound **13** demonstrated a marginal increase in enzyme affinity for Aurora A and 10-fold increase for Aurora B. Of these compounds, the 2,6-difluorophenyl analogue **12** was chosen for further profiling and demonstrated potent inhibition of HCT116 colony formation (IC$_{50}$ = 17 nM)[36] in the secondary cellular assay. Compound **12** was also found to have reduced plasma protein binding (PPB = 83.1%).

Further work then focused on identifying compounds with an attractive in vitro profile similar to **12**, but with reduced lipophilicity (log $D_{7.4}$ of **12** = 3.1). Although minimizing lipophilicity offers no guarantees in terms of avoiding poor ADMET properties, it is widely accepted that minimizing log *P* is broadly associated with reduced attrition rates during clinical development.[38,39] Analogues containing more polar heterocycles retained respectable activity in the enzyme assay but demonstrated reduced cellular potency, as exemplified by the 3-pyridyl analogue **14** (polyploidy at 1−3 μM) and the 4-tetrahydropyranyl analogue **15** (polyploidy at 1 μM). An alternative strategy to reduce lipophilicity, based on cyclohexyl analogue **13**, relied on reducing the size of the hydrophobic cyclohexane motif rather than introducing heteroatoms. Gratifyingly, this approach demonstrated that high enzyme and cellular potency could be

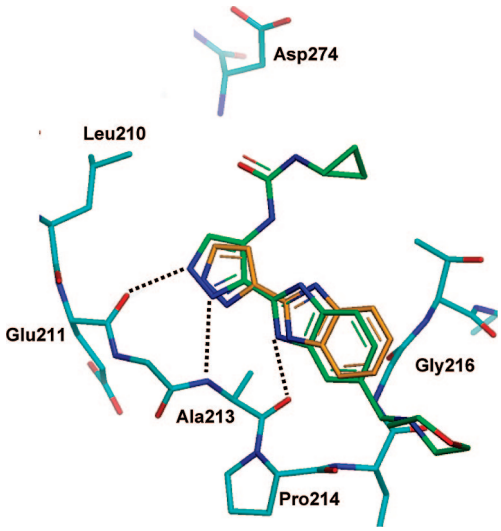

Figure 4. Crystal structure of **16** (green) complexed with Aurora A (blue) superimposed with the binding mode of fragment **5** (orange) (without associated protein structure).

Table 3. Molecular Profile of Compound **16**

protein	IC_{50} (nM)
Aurora A	52% I at 3.0 nM
Aurora B	58% I at 3.0 nM
JAK3	1.1
JAK2	1.2
Abl (T315I)	4
GSK3-β, FGFR2, VEGFR3 (Flt4), Mer, Ret, Rsk2, Rsk3, Tyk2, Yes	1−10
Abl(Q252H), DRAK1, FGFR1, FGFR1(V561M), FGFR2(N549H), FGFR3, VEGFR1(Flt1), Flt-3, PDGFR-α(D842V), PDK1, PKCμ, Rsk4, SRC(T341M), VEGFR2	10−30
21 kinases	30−100
37 kinases	100−300
144 kinases	>300

maintained while reducing both MW and lipophilicity as exemplified by the cyclopropyl urea **16** (log $D_{7.4} = 2.1$, MW = 381). Although compound **16** (Aurora A $IC_{50} \approx 3$ nM, LE ≈ 0.42) proved too potent for an accurate IC_{50} value to be measured in the available assay format, HCT116 cells treated with this compound (0.03 μM) demonstrated a clear polyploid phenotype. Furthermore, **16** demonstrated potent inhibition of HCT116 colony formation (IC_{50} = 12 nM) in the secondary cellular assay, a clean CYP450 profile (IC_{50} > 10 μM for CYP3A4, 2D6, 1A2, 2C9, 2C19), acceptable mouse plasma protein binding (81.5%) and good thermodynamic solubility (2.0 mg/mL at pH7.0 and 13 mg/mL at pH5.5).

The crystal structure of compound **16** complexed with Aurora A is shown in Figure 4. As with the initial urea analogue **10**, the urea linker adopts a cis/trans configuration that results in the molecule having a folded conformation. This same conformation was also observed in the crystal structure of **16** alone (Figure 5a) and in DMSO solution as confirmed by NMR (Figure 5b). An NOE was observed between H3b/H3b′ of the cyclopropyl ring and the H4 and H7 protons of the benzimidazole ring. These data, taken together, suggest that this folded conformation may be stabilized by a hydrophobic interaction between these two groups.

Figure 4 also serves to illustrate that the key hydrogen bonding interactions between initial fragment **5** and Aurora A are retained in the case of compound **16**. This is consistent with the concept that fragments, while only having modest affinity, can be considered to be efficient ligands that make strong interactions with the target protein. This case adds to the growing number of literature examples where the fragment−protein interactions are maintained throughout the optimization process and are ultimately retained in final compounds.[6] In the case of compound **16**, the good ligand efficiency of **5** (Aurora A IC_{50} = 0.91 μM, LE = 0.59) and the decision to retain the pyrazole-benzimidazole motif created a high probability of achieving low nanomolar potency while keeping well within the molecular weight and lipophilicity guidelines for drug-likeness.[38−40]

Biological Profile of 16. In a cross-screen against other kinases, compound **16** demonstrated activity against other enzymes that have been suggested as targets for anticancer therapy, including JAK2, Flt-3, and Abl (T315I) (Table 3). This can be understood structurally. It is proposed that the benzimidazole motif of **16** binds to a region of these kinases that shares close structural similarity with Aurora A. This was confirmed in the case of JAK2 by the X-ray crystallographic structure of this enzyme complexed with compound **16** (Figure 6). As in Aurora A, the hinge region of JAK2 contains an extra glycine residue (Gly935), relative to the CDKs, which leads to the pocket having a particular affinity for flat aromatic heterocyles such as benzimidazole. This glycine residue is common to other kinases with a strong affinity for compound **16** such as Flt-3 and Abl (T315I) (Table 4).

Analysis of Table 4 suggests that the binding of compound **16** is relatively insensitive to the nature of the gatekeeper residue. This is in contrast to other classes of compound such as the Abl kinase inhibitor **17** (imatinib, Figure 7). In Abl (T315I), a more sterically demanding isoleucine gatekeeper residue prevents the binding of **17**, which typically projects beyond the gatekeeper, but does not prevent binding of compound **16** which binds exclusively to the ATP pocket.

As a result of the complex signaling network associated with kinases, multitargeted kinase inhibitors may offer advantages in the treatment of cancer. The possibilities presented by the additional interesting activities of **16** will be the subject of future publications.

On the basis of the good balance between in vitro potency and physicochemical properties, compound **16** was chosen for further studies in vivo. Following intravenous (iv) dosing to HCT116 xenograft bearing mice, **16** demonstrated a significantly longer half-life in tumors compared with plasma (Table 5). The compound was also found to possess modest oral bioavailability in mice (F_{po} = 24%) in spite of relatively high plasma clearance. Interestingly, incubation of **16** with mouse hepatocytes in vitro (clearance = 8.8 (μM/min)/million cells) was predictive of only modest clearance in vivo, suggesting that a mechanism other than hepatic clearance may be involved. Overall, this profile was considered suitable for development of **16** as an iv agent with the potential for oral administration.

Compound **16** was evaluated for its in vivo antitumor activity in immunocompromised BALB/c nude mice bearing early stage HCT116 human colon carcinoma xenografts (Figure 8). In this study, the hydrochloride salt of **16** was administered via the intraperitoneal route (ip) on an intermittent dosing schedule. Doses of 15 and 20 mg/kg were seen to produce a significant tumor growth inhibition of 67% (% *T/C* = 33%) and 76% (% *T/C* = 24%), respectively (on day 16 of the treatment). These doses were well tolerated with mean body weight being maintained above 90% relative to the starting weight. A more extensive in vivo efficacy evaluation, including PK/PD and cell cycle analysis, will be published separately.

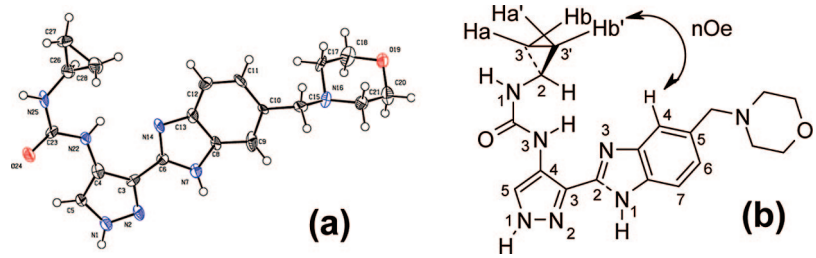

Figure 5. (a) X-ray crystal structure of compound **16** alone. (b) Conformation of **16**, based NOE observations (NMR, DMSO-d_6). See Supporting Information for detailed experimental methods.

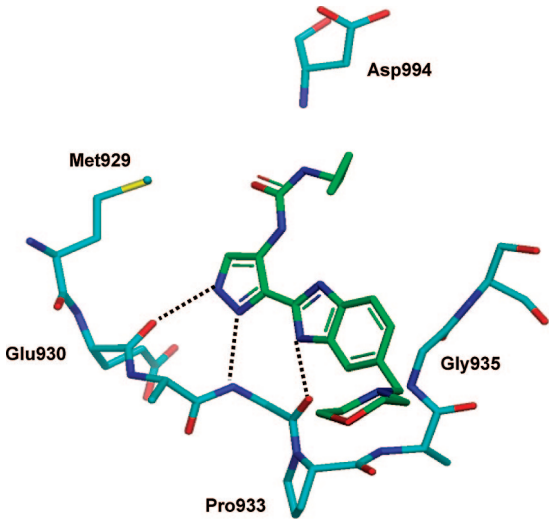

Figure 6. Crystal structure of compound **16** complexed with JAK2.

Table 4. Amino Acid Sequences for the Five Kinase Hinge Regions[a]

Aurora A	gatekeeper, *210*	211	212	213	214	215	inserted Gly, **216**	217
Aurora A	*L*	E	Y	A	P	L	**G**	T
JAK2	*M*	E	Y	L	P	Y	**G**	S
Abl (T315I)	*I*	E	F	M	T	Y	**G**	N
Flt-3	*F*	E	Y	C	C	Y	**G**	D
CDK2	*F*	E	F	L	H	Q		D

[a] Residue numbering refers to Aurora A. The glycine residues (conserved in Aurora A, JAK2, Abl (T315I), Flt-3 but absent in CDK2) are in boldface. The gatekeeper residues are italicized.

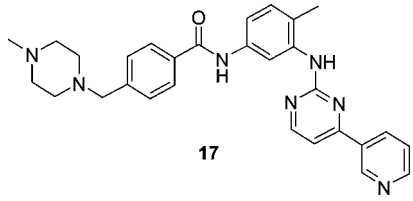

Figure 7

Chemistry. Compounds **8**−**16** were synthesized as described in Scheme 2. Treatment of 3,4-dinitrobenzoic acid **18** with $SOCl_2$, followed by morpholine, afforded the amide **19**. Reduction of the amide was achieved using $NaBH_4$ in the presence of Lewis acid $BF_3 \cdot OEt_2$ to give the dinitrobenzene **20**. Palladium catalyzed hydrogenation then gave the diamine **21**. The benzimidazole **22** was constructed by first coupling the diamine **21** with 4-nitro-1*H*-pyrazole-3-carboxylic acid followed by heating in AcOH. Subsequent palladium catalyzed hydrogenation then afforded the aminopyrazole **23**. Final compounds **8**−**16** were then prepared from **23**, using standard methods for amide or urea formation. Compounds **6** and **7** were prepared in an analogous fashion to compound **8** but using *o*-phenylenediamine instead of diamine **21**.

Conclusions

The pyrazole-benzimidazole **5** was identified during the course of a CDK program as a ligand efficient fragment starting point for the discovery of Aurora kinase inhibitors. X-ray crystallographic structures were generated using a novel soakable form of Aurora A and were used to drive the optimization toward potent ($IC_{50} \approx 3$ nM) dual Aurora A/Aurora B inhibitors. These compounds inhibited growth and survival of HCT116 cells and produced the polyploid cellular phenotype typically associated with Aurora B kinase inhibition. Optimization of cellular activity and physicochemical properties ultimately led to the identification of **16** (AT9283). In addition to Aurora A and Aurora B, **16** was also found to inhibit a number of other kinases including JAK2, Flt3, and Abl (T315I) ($IC_{50} = 1-30$ nM). Compound **16** demonstrated in vivo efficacy in mouse xenograft models and was selected for preclinical development. This compound has advanced into phase I clinical trials for the treatment of cancer.[41]

Experimental Section

Protein Crystallography. Phosphorylated Aurora A kinase was produced as described by Bayliss et al.[42] Apo protein was concentrated to ~10 mg/mL, and crystals were grown using the hanging drop vapor diffusion method. Crystals were grown from conditions containing 100 mM Na_2HPO_4/KH_2PO_4, pH 6.2, 14−19% ethylene glycol and by mixing equal volumes of protein and well solution. Crystals appeared within 2 days. Cross-validation of both the soakable and cocrystallization systems was performed with known ligands and showed that ligand binding modes were the same in each case. Crystal structures of compounds bound to CDK2 were obtained following methods described previously.[13]

Aurora A and Aurora B Kinase Assays. Assays for Aurora A and B were performed in a DELFIA format. Aurora A enzyme was incubated with test compound and 3 μM cross-tide substrate (biotin-CGPKGPGRRGRRRTSSFAEG) in 10 mM MOPS, pH 7, 0.1 mg/mL BSA, 0.001% Brij-35, 0.5% glycerol, 0.2 mM EDTA, 10 mM $MgCl_2$, 0.01% β-mercaptoethanol, 15 μM ATP, and 2.5% DMSO. Aurora B enzyme was incubated with test compound, 3 μM of the above substrate in 25 mM Tris, pH 8.5, 5 mM $MgCl_2$, 0.1 mg/mL BSA, 0.025% Tween-20, 1 mM DTT, 15 μM ATP, and 2.5% DMSO. Reactions were allowed to proceed for 60 min and 45−90 min for Aurora A and Aurora B, respectively, before quenching with EDTA. The reaction mixtures were then transferred to a neutravidin-coated plate, and phosphorylated peptide was quantified by means of a phospho-specific antibody (Cell Signalling Technology) and a europium labeled secondary antibody (Perkin-Elmer) using time-resolved fluorescence (excitation, 337 nm; emission, 620 nm). IC_{50} values for the control compounds were 92 ± 19 nM (Aurora A assay, $n = 51$) and 17 ± 7.3 nM (Aurora B, $n = 14$).

Primary HCT116 Cellular Assay. HCT 116 cells were cultured in DMEM + 10% FBS + GLUTAMAX I. Black 96-well flat-

Table 5. Pharmacokinetic Data for Compound **16** after Administration to BALB/c Mice

plasma protein binding (mouse) (%)[a]	clearance ((mL/min)/kg)	V_{ss} (L/kg)[b]	$T_{1/2}$ (h)	C_{max} (μM)	AUC_{0-t} (μM·h)	F (%)
81.5	114[b]	3.9[b]	0.5 (plasma)[b] 2.5 (tumor)[c]	4.9 (iv)[b] 0.45 (po)[d] 8.4 (ip)[e]	1.9 (iv)[b] 0.91 (po)[d] 7.7 (ip)[e]	24 (po)[d] 100 (ip)[e]

[a] Mouse plasma using equilibrium dialysis ($n = 6$). [b] Value determined following intravenous (iv) administration at 5 mg/kg. [c] Mean value determined following IV administration at 10 mg/kg ($n = 2$). [d] Determined following oral (po) dosing at 10 mg/kg. [e] Determined following intraperitoneal (ip) dosing at 20 mg/kg. Absorption was essentialy complete.

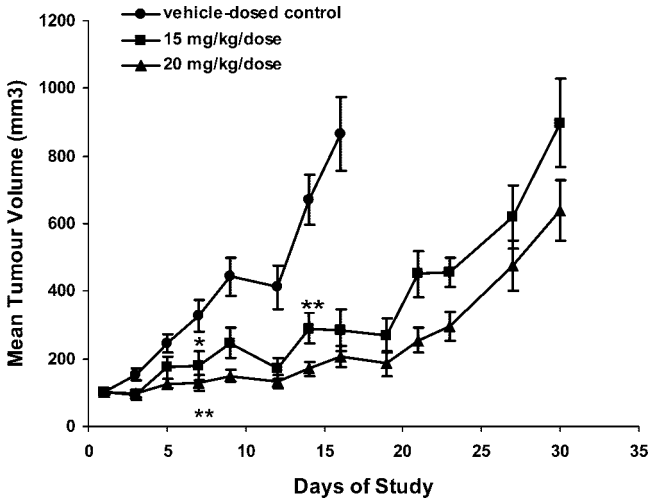

Figure 8. Efficacy of **16** in the early stage HCT116 colon carcinoma cell line xenograft mouse model following intermittent administration at 15 and 20 mg/kg twice daily (b.i.d. × 2, q4d) given by the intraperitoneal route for 18 days (five cycles) against a matched vehicle-dosed control. Results shown indicate mean tumor volume ± SEM for groups of $n = 8$. Growth curves became significantly different from control from day 7 onward (**, $p < 0.001$; *, $p < 0.05$).

bottomed (clear) tissue culture treated plates were seeded at 5×10^3 cells per well in 200 μL of medium and incubated for approximately 16 h at 37 °C in a humidified atmosphere of 5% CO_2 in air. Cells were treated with test compound at nine different concentrations (spanning 1 nM to 10 μM, plus DMSO vehicle control) and then incubated for 72 h. Polyploidy morphological observations of the cells were then noted. The concentration of test compound required to produce a distinct polyploid phenotype was reported.

HCT116 Colony Forming Assay (Secondary Assay). Cells were seeded at a concentration of 75−100 cells/mL relevant culture media onto 6- or 24-well tissue culture plates and allowed to recover for 16 h. Test compound (11 concentrations spanning 0.1 nM to 10 μM) or vehicle control (DMSO) was added to duplicate wells to give a final DMSO concentration of 0.1%. Following compound addition, colonies were allowed to grow between 10 and 14 days for optimum discrete colony counting. Colonies were fixed in 2 mL of Carnoys fixative (25% acetic acid, 75% MeOH) and stained in 2 mL of 0.4% w/v crystal violet. The numbers of colonies in each well was counted. IC_{50} values were calculated by sigmoidal dose-response (variable slope) IC_{50} curves using Prism Graphpad software.

Pharmacokinetic and Tumor Distribution Study Method. Detailed pharmacokinetic parameters were determined after administration of a single dose of compound **16** (hydrochloride salt) to BALB/c mice. Distribution studies were carried out using immunocompromised BALB/c mice bearing HCT116 tumors. Tumour and/or plasma samples were collected at timed intervals following iv dosing at either 5 or 10 mg/kg (100% saline), ip dosing at 20 mg/kg [10% DMSO, 20% water, 70% hydroxypropyl-β-cyclodextrin (25% w/v aq)] or oral dosing at 10 mg/kg (10% saline, 90% water). All tumor samples were homogenized in 5 volumes (w/v) of acetonitrile/water (50/50). Quantitative analysis was performed as described in the Supporting Information.

Efficacy Study in the HCT116 Colon Carcinoma Cell Line Xenograft Model. The investigation was performed in a xenograft mouse model derived from HCT116 cell suspension inoculated subcutaneously (sc) in the hind flank of male BALB/c mice (Hsd, athymic nude-Foxn1^{nu}; Harlan UK, Bicester, U.K.) which were allowed to grow to approximately 100 mm^3. Mice were then dosed with compound **16** [10% DMSO, 20% water, 70% hydroxypropyl-β-cyclodextrin (25% w/v aq)] twice daily for 2 days and not dosed for 2 days, and then the cycle was repeated five times [15 and 20 mg/kg twice daily (b.i.d. × 2, q4d) × 5]. Tumor dimensions were recorded every 2 or 3 days using external measurements, and the tumor volume was calculated using the equation for an ellipsoid (length × width^2/2). Animals in the control group received dose vehicle only on the same schedule. Estimates of growth inhibition and %T/C values were derived from the resulting growth curves.

Chemistry. Reagents and solvents were obtained from commercial suppliers and used without further purification. Thin layer chromatography (TLC) analytical separations were conducted with E. Merck silica gel F-254 plates of 0.25 mm thickness and were visualized with UV light (254 nM) and/or stained with iodine, potassium permanganate or phosphomolybdic acid solutions followed by heating. Standard silica gel (SiO_2) column chromatography was employed as a method of purification using the indicated solvent mixtures. Compound purification was also carried out using a Biotage SP4 system using prepacked disposable SiO_2 cartridges (4, 8, 19, 38, 40, and 90 g sizes) with stepped or gradient elution at 5−40 mL/min of the indicated solvent mixture. Proton nuclear magnetic resonance (^{1}H NMR) spectra were recorded in the deuterated solvents specified on a Bruker Avance 400 spectrometer operating at 400 MHz. Chemical shifts are reported in parts per million (δ) from the tetramethylsilane internal standard. Data are reported as follows: chemical shift, multiplicity (br = broad, s = singlet, d = doublet, t = triplet, m = multiplet), coupling constants (Hz), integration. Compound purity and mass spectra were determined using an Agilent 1200SL-6140 LC/MS with an Acquity UPLC BEH C18 column, eluting with a 5−95% gradient of CH_3CN (elutant B) and 10 mM aqueous (NH_4HCO_3 + NH_4OH)/CH_3CN (95:5) (elutant A). Reverse phase preparative LC/MS was performed on a Waters Fractionlynx system using either a Phenomenex Synergy MAX-RP or a Phenomenex Luna C18 (2) column (see Supporting Information for detailed experimental information).

(3,4-Dinitrophenyl)morpholin-4-ylmethanone (19). A solution of 3,4-dinitrobenzoic acid **18** (10 g, 47 mmol) and DMF (0.1 mL) in THF (100 mL) was treated with thionyl chloride (4.5 mL, 62 mmol) and then heated at reflux for 2.5 h. The mixture was then cooled to ~0 °C, and triethylamine (10 mL, 71 mmol) was added over 20 min, keeping the internal temperature at <5 °C. Morpholine (7.2 mL, 82 mmol) was added over 15 min, keeping the internal temperature at <10 °C, and then the mixture was allowed to warm to ambient temperature. After being stirred overnight, the mixture was diluted with water (250 mL) and cooled in ice. A beige solid was filtered off under suction, washed with a further portion of cold water (25 mL), and dried in vacuo to afford **19** as a yellow solid (12.7 g, 96%). ^{1}H NMR (400 MHz, DMSO-d_6): 8.33−8.29 (m, 2H), 8.01 (d, $J = 8.2$ Hz, 1H), 3.73−3.63 (m, 4H), 3.35−3.30 (m, 4H). LC/MS: $t_R = 1.08$ min, $m/z = 282$ $[M + H]^+$.

4-(3,4-Dinitrobenzyl)morpholine (20). Sodium borohydride (3.36 g, 89 mmol) was ground, placed in a nitrogen-flushed flask and suspended in THF (120 mL). After the mixture was cooled to ~0 °C, boron trifluoride etherate (11.3 mL, 89 mmol) was added

Scheme 2[a]

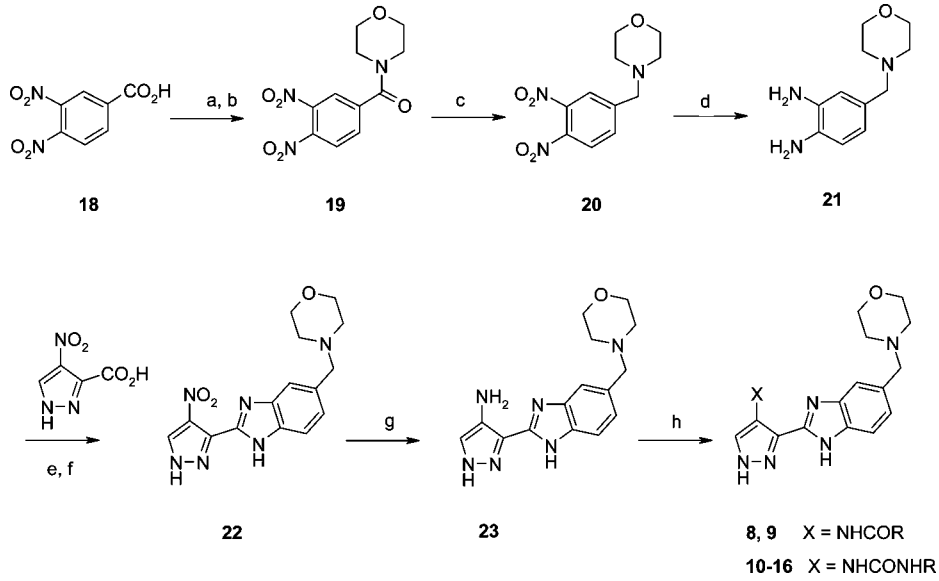

[a] Reagents and conditions: (a) $SOCl_2$, THF, DMF; (b) morpholine, THF, Et_3N; (c) $NaBH_4$, $BF_3.OEt_2$, THF; (d) 10% Pd−C, H_2, EtOH; (e) EDC, HOBt, DMF; (f) AcOH, reflux; (g) 10%Pd−C, H_2, DMF; (h) standard amide and urea coupling methods (see *Experimental Section* for specific reagents).

via syringe. This reaction is mildly exothermic, and some hydrogen evolution was noted. (3,4-Dinitrophenyl)morpholin-4-ylmethanone **19** (11.91 g, 42 mmol) was added as a solid in one portion. Cooling was removed and the suspension stirred at room temperature for 3 h before cooling again in ice. MeOH (100 mL) was added cautiously (hydrogen evolution), and then the mixture was brought to reflux for 1 h. The mixture was concentrated in vacuo, and then the residue was partitioned between EtOAc (100 mL) and 1:1 saturated $NaHCO_3$ solution/water (100 mL). The organic phase was separated, washed with water (50 mL) and then brine (100 mL), and dried ($MgSO_4$). The initial $NaHCO_3$ wash was extracted a second time with EtOAc (50 mL), this extract then being washed with the same aqueous washes used for the first extract before drying ($MgSO_4$), combination, and concentration to afford 10.97 g of crude material. Recrystallization from MeOH (45 mL) gave **20** (9.34 g, 83%). ^{1}H NMR (400 MHz, Me-d_3-OD): 8.08−9.03 (m, 2H), 7.87 (d, J = 8.2 Hz, 1H), 3.75−3.69 (m, 6H), 2.54−2.50 (m, 4H). LC/MS: t_R = 1.22 min, m/z = 268 $[M + H]^+$.

4-Morpholin-4-ylmethylbenzene-1,2-diamine (21). 10% palladium on carbon (1.05 g) and 4-(3,4-dinitrobenzyl)morpholine **20** (21 g, 101 mmol) were suspended in EtOH (900 mL) under nitrogen. The mixture was cooled in ice and then the atmosphere exchanged for hydrogen. The mixture was allowed to warm to 15−20 °C, and hydrogenation continued at ambient pressure for 2 days. The vessel was purged with nitrogen. Then the mixture was filtered through Celite, rinsing with EtOH (300 mL) in portions. Concentration afforded **21** (15.8 g, 97%). ^{1}H NMR (400 MHz, DMSO-d_6): 6.49−6.43 (m, 1H), 6.42 (d, J = 7.7 Hz, 1H), 6.29 (d, J = 7.7 Hz, 1H), 4.35 (br, 4H), 3.55−3.52 (m, 4H), 3.19 (s, 2H), 2.31−2.26 (m, 4H).

5-Morpholin-4-ylmethyl-2-(4-nitro-1*H*-pyrazol-3-yl)-1*H*-benzimidazole (22). A mixture of 4-morpholin-4-ylmethyl-benzene-1,2-diamine **21** (2.30 g, 11.1 mmol), 4-nitro-1*H*-pyrazole-3-carboxylic acid (1.57 g, 10.0 mmol), EDC (2.13 g, 11.1 mmol), and HOBt (1.50 g, 11.1 mmol) in dry DMF (25 mL) was stirred at ambient temperature for 24 h. The mixture was reduced in vacuo and the crude residue dissolved in AcOH (40 mL) and heated at reflux for 3 h. The solvent was removed in vacuo and the residue was purified by SiO_2 column chromatography, eluting with 0−20% MeOH in EtOAc to give nitropyrazole **22** as a yellow solid (1.0 g, 61%). ^{1}H NMR (400 MHz, Me-d_3-OD): 8.68 (s, 1H), 7.71−7.65 (m, 2H), 7.38 (d, J = 8.3 Hz, 1H), 3.75−3.71 (m, 6H), 2.59−2.54 (m, 4H). LC/MS: t_R = 1.83 min, m/z = 329 $[M + H]^+$.

3-(5-morpholin-4-ylmethyl-1*H*-benzimidazol-2-yl)-1*H*-pyrazol-4-ylamine (23). 10% palladium on carbon (0.08 g) was added to the nitropyrazole **22** (0.82 g, 2.5 mmol) in DMF (30 mL) under an atmosphere of nitrogen. The mixture was shaken under a hydrogen atmosphere for 4 h and then filtered through Celite, washing with MeOH. The filtrate was concentrated in vacuo to give **23** as a brown solid (530 mg, 71%), which was used without further purification. ^{1}H NMR (400 MHz, Me-d_3-OD): 7.60−7.54 (m, 2H), 7.34 (s, 1H), 7.25 (d, J = 7.7 Hz, 1H), 3.74−3.70 (m, 4H), 3.66 (s, 2H), 2.55−2.49 (m, 4H). LC/MS: t_R = 0.91 min, m/z = 299 $[M + H]^+$.

***N*-[3-(5-Morpholin-4-ylmethyl-1*H*-benzoimidazol-2-yl)-1*H*-pyrazol-4-yl]benzamide (8).** To a solution of aminopyrazole **23** (100 mg, 0.33 mmol) and diisopropylethylamine (130 μL, 0.73 mmol) in THF (3 mL) was added benzoyl chloride (78 μL, 0.66 mmol). After the mixture was stirred for 3 h, 1.5 mL of 1 N KOH/MeOH solution was added and the mixture stirred for a further 16 h. The mixture was concentrated in vacuo and the residue partitioned between EtOAc and water. The organic layer was washed with brine and dried ($MgSO_4$) and the residue purified by preparative LC/MS to give **8** as the formic acid salt (48 mg, 31%). ^{1}H NMR (400 MHz, Me-d_3-OD): 8.40 (s, 1H), 8.37 (s, 1H), 8.16−8.11 (m, 2H), 7.74 (s, 1H), 7.70−7.61 (m, 4H), 7.34 (d, J = 8.2 Hz, 1H), 4.00 (s, 2H), 3.82−3.77 (m, 4H), 2.88−2.81 (m, 4H). LC/MS: t_R = 1.26 min, m/z = 403 $[M + H]^+$.

1-[3-(5-Morpholin-4-ylmethyl-1*H*-benzoimidazol-2-yl)-1*H*-pyrazol-4-yl]-3-phenylurea (10). To aminopyrazole **23** (100 mg, 0.33 mmol), in THF (2 mL), was added phenyl isocyanate (72 μL, 0.66 mmol), and the mixture was stirred for 16 h at ambient temperature. Resin-supported tris-amine (800 mg, 4 mmol/g) was added and the mixture agitated for a further 4 h. The resin was removed by filtration, the filtrate was treated with 1 N KOH (2 mL, MeOH/THF; 1:3), and the solution was stirred for approximately 16 h. The mixture was then partitioned between EtOAc and H_2O. The organic layer was then washed with brine, dried ($MgSO_4$), and evaporated to dryness. The crude solid was dissolved in DCM and triturated with hexanes to give a solid that was collected by filtration. Purification by SiO_2 column chromatography, eluting with 0−20% MeOH in EtOAc, gave **10** (45 mg, 32%). ^{1}H NMR (400 MHz, Me-d_3-OD): 8.15 (s, 1H), 7.75−7.67 (m, 1H), 7.54−7.49 (m, 3H), 7.34 (t, J = 7.6 Hz, 2H), 7.28 (d, J = 8.7 Hz, 1H), 7.08 (t, J = 7.4 Hz, 1H), 3.75−3.71 (m, 4H), 3.69 (s, 2H), 2.54 (s, 4H). LC/MS: t_R = 1.19 min, m/z = 418 $[M + H]^+$.

1-Cyclopropyl-3-[3-(5-morpholin-4-ylmethyl-1*H*-benzoimidazol-2-yl)-1*H*-pyrazol-4-yl]urea (16). A mixture of aminopyrazole **23** (10.96 g, 36.8 mmol) and CDI (11.7 g, 72.2 mmol) in THF (200 mL) was heated at reflux for ~16 h. The mixture was allowed to cool, and the resulting precipitate was collected by filtration, washed with THF, and dried in vacuo. The material was combined with cyclopropylamine (17 mL) and DMF (50 mL) and then the mixture heated at 100 °C for 16 h. The mixture was then allowed to cool and concentrated in vacuo. The residue was purified by SiO_2 column chromatography, eluting with 2−20% MeOH in EtOAc, to give a **16** as a pale-yellow solid (8.19 g, 87%). ^{1}H NMR (400 MHz, Me-d_3-OD): 8.07 (s, 1H), 7.58 (s, 2H), 7.26 (d, J = 8 Hz, 1H), 3.74−3.69 (m, 4H), 3.67 (s, 2H), 2.74−2.69 (m, 1H), 2.55−2.50 (m, 4H), 1.02−0.93 (m, 2H), 0.72−0.65 (m, 2H). LC/MS: t_R = 1.08 min, m/z = 382 $[M + H]^+$.

1-Cyclopropyl-3-[3-(5-morpholin-4-ylmethyl-1*H*-benzoimidazol-2-yl)-1*H*-pyrazol-4-yl]urea (16), Hydrochloride Salt. Compound **16** (2.05 g, 5.37 mmol) was dissolved in MeOH/EtOAc (1:10, 100 mL) and treated with 4 N HCl in dioxane (1.48 mL, 5.91 mmol). The resulting precipitate was collected by filtration and dried to give **16** as the monohydrochloride salt (1.5 g, 67%). ^{1}H NMR (400 MHz, DMSO-d_6): 13.26−13.07 (m, 2H), 11.05−10.80 (m, 1H), 9.64 (s, 1H), 8.08 (s, 1H), 7.98−7.19 (4H, m), 4.44 (s, 2H), 3.94 (d, J = 12.4 Hz, 2H), 3.77 (t, J = 12.3 Hz, 2H), 3.28−3.20 (m, 2H), 3.17−3.05 (m, 2H), 2.65−2.57 (m, 1H), 0.96−0.79 (m, 2H), 0.63−0.51 (m, 2H).

Acknowledgment. The authors thank Neil Thompson, Chris Murray, Jeff Yon, Michelle Jones, Nicola Wallis, and Miles Congreve for advice and useful discussion. We also acknowledge Harren Jhoti and Robin Carr for their support throughout this work. We are also grateful to Douglas Ross for the measurement of plasma protein binding, Cesare Granata for both analytical and preparative HPLC support, Hayley Angove, Caroline Richardson, and Lisa Seavers for biology support, Margaret Walker, Nick Davies, and Gary Trewartha for synthetic chemistry support, and Martyn Frederickson for proofreading.

Supporting Information Available: Detailed descriptions of HPLC methods; HPLC purity analysis of final compounds; synthetic procedures and spectral data for compounds **9** and **11**−**15**; experimental details for other biological assays and DMPK studies. This material is available free of charge via the Internet at http://pubs.acs.org.

References

(1) Erlanson, D. A.; McDowell, R. S.; O'Brien, T. Fragment-based Drug Discovery. *J. Med. Chem.* **2004**, *47*, 3463–3482.
(2) Rees, D. C.; Congreve, M.; Murray, C. W.; Carr, R. Fragment-Based Lead discovery. *Nat. Rev. Drug Discovery* **2004**, *3* (8), 660–672.
(3) Ciulli, A.; Abell, C. Fragment-Based Approaches to Enzyme Inhibition. *Curr. Opin. Biotechnol.* **2007**, *18*, 489–496.
(4) Hajduk, P. J.; Greer, J. A Decade of Fragment-based Drug Design: Strategic Advances and Lessons Learned. *Nat. Rev. Drug Discovery* **2007**, *6*, 211–219.
(5) Congreve, M.; Murray, C. W.; Carr, R.; Rees, D. C. *Annual Reports in Medicinal Chemistry*; Elsevier, Inc.: New York, 2007; pp 431−448.
(6) Congreve, M.; Chessari, G.; Tisi, D.; Woodhead, A. J. Recent Developments in Fragment-based Drug Discovery. *J. Med. Chem.* **2008**, *51* (13), 3661–3680.
(7) Hartshorn, M. J.; Murray, C. W.; Cleasby, A.; Frederickson, M.; Tickle, I. J.; Jhoti, H. Fragment-Based Lead Discovery Using X-ray Crystallography. *J. Med. Chem.* **2005**, *48* (2), 403–413.
(8) Lesuisse, D.; Lange, G.; Deprez, P.; Bernard, D.; Schoot, B.; Delettre, G.; Marquette, J. P.; Broto, P.; Jean-Baptiste, V.; Bichet, P.; Sarubbi, E.; Mandine, E. SAR and X-ray. A New Approach Combining Fragment-Based Screening and Rational Drug Design: Application to the Discovery of Nanomolar Inhibitors of Src SH2. *J. Med. Chem.* **2002**, *45*, 2379–2387.
(9) Lepre, C. A.; Moore, J. M.; Peng, J. W. Theory and Applications of NMR-Based Screening in Pharmaceutical Research. *Chem. Rev.* **2004**, *104*, 3641–3676.
(10) Neumann, T.; Junker, H. D.; Schmidt, K.; Sekul, R. SPR-Based Fragment Screening: Advantages and Applications. *Curr. Top. Med. Chem.* **2007**, *7*, 1630–1642.
(11) Hopkins, A. L.; Groom, C. R.; Alex, A. Ligand Efficiency: A Useful Metric for Lead Selection. *Drug Discovery Today* **2004**, *9*, 430–431.
(12) Abad-Zapatero, C.; Metz, J. T. Ligand Efficiency Indices as Guideposts for Drug Discovery. *Drug Discovery Today* **2005**, *10*, 464–467.
(13) Wyatt, P. G.; Woodhead, A. J.; Berdini, V.; Boulstridge, J. A.; Carr, M. G.; Cross, D. M.; Davis, D. J.; Devine, L. A.; Early, T. R.; Feltell, R. E.; Lewis, E. J.; McMenamin, R. L.; Navarro, E. F.; O'Brien, M. A.; O'Reilly, M.; Reule, M.; Saxty, G.; Seavers, L. C. A.; Smith, D.-M.; Squires, M. S.; Trewartha, G.; Walker, M. T.; Woolford, A. J.-A. Identification of N-(4-Piperidinyl)-4-(2,6-dichlorobenzoylamino)-1H-pyrazole-3-carboxamide (AT7519), a Novel Cyclin Dependent Kinase Inhibitor Using Fragment-Based X-Ray Crystallography and Structure Based Drug Design. *J. Med. Chem.* **2008**, *51* (16), 4986–4999.
(14) Carmena, M.; Earnshaw, W. C. The Cellular Geography of Aurora Kinases. *Nat. Rev. Mol. Cell Biol* **2003**, *4* (11), 842–854.
(15) Gautschi, O.; Heighway, J.; Mack, P. C.; Purnell, P. R.; Lara, P. N., Jr.; Gandara, D. R. Aurora Kinases as Anticancer Drug Targets. *Clin. Cancer Res* **2008**, *14* (6), 1639–1648.
(16) Sen, S.; Zhou, H.; White, R. A. A Putative Serine/Threonine Kinase Encoding Gene BTAK on Chromosome 20q13 Is Amplified and Overexpressed in Human Breast Cancer Cell Lines. *Oncogene* **1997**, *14* (18), 2195–2200.
(17) Bischoff, J. R.; Anderson, L.; Zhu, Y.; Mossie, K.; Ng, L.; Souza, B.; Schryver, B.; Flanagan, P.; Clairvoyant, F.; Ginther, C.; Chan, C. S.; Novotny, M.; Slamon, D. J.; Plowman, G. D. A Homologue of Drosophila Aurora Kinase Is Oncogenic and Amplified in Human Colorectal Cancers. *EMBO J.* **1998**, *17* (11), 3052–3065.
(18) Katayama, H.; Ota, T.; Jisaki, F.; Ueda, Y.; Tanaka, T.; Odashima, S.; Suzuki, F.; Terada, Y.; Tatsuka, M. Mitotic Kinase Expression and Colorectal Cancer Progression. *J. Natl. Cancer Inst.* **1999**, *91* (13),), 1160–1162.
(19) Kamada, K.; Yamada, Y.; Hirao, T.; Fujimoto, H.; Takahama, Y.; Ueno, M.; Takayama, T.; Naito, A.; Hirao, S.; Nakajima, Y. Amplification/Overexpression of Aurora-A in Human Gastric Carcinoma: Potential role in differentiated type gastric carcinogenesis. *Oncol. Rep.* **2004**, *12* (3), 593–599.
(20) Giet, R.; Petretti, C.; Prigent, C. Aurora Kinases, Aneuplody and Cancer, a Coincidence or a Real Link? *Trends Cell Biol.* **2005**, *15*, 241–250.
(21) Mortlock, A.; Keen, N. J.; Jung, F. H.; Heron, N. M.; Foote, K. M.; Wilkinson, R.; Green, S. Progress in the Development of Selective Inhibitors of Aurora Kinases. *Curr. Top. Med. Chem.* **2005**, *5*, 199–213.
(22) Warner, S. L.; Bashyam, S.; Vankayalapati, H.; Bearss, D. J.; Han, H.; Von Hoff, D. D.; Hurley, L. H. Identification of a Lead Small-Molecule Inhibitor of the Aurora Kinases Using a Structure-Assisted, Fragment-Based Approach. *Mol. Cancer Ther.* **2006**, *5*, 1764–1773.
(23) Cancilla, M. T.; He, M. M.; Viswanathan, N.; Simmons, R. L.; Taylor, M.; Fung, A. D.; Cao, K.; Erlanson, D. A. Discovery of an Aurora Kinase Inhibitor through Site-Specific Dynamic Combinatorial Chemistry. *Bioorg. Med. Chem. Lett.* **2008**, *18*, 3978–3981.
(24) Ditchfield, C.; Johnson, V. L.; Tighe, A. E. R.; Haworth, C.; Johnson, T.; Mortlock, A.; Keen, N.; Taylor, S. S. Aurora B Couples Chromosome Alignment with Anaphase by Targeting BubR1, Mad2, and Cenp-E to Kinetochores. *J. Cell Biol.* **2003**, *161* (2), 267–280.
(25) Soncini, C.; Carpinelli, P.; Gianellini, L.; Fancelli, D.; Vianello, P.; Rusconi, L.; Storici, P.; Zugnoni, P.; Pesenti, E.; Croci, V.; Ceruti, R.; Giorgini, M. L.; Cappella, P.; Ballinari, D.; Sola, F.; Varasi, M.; Bravo, R.; Moll, J. PHA-680632, a Novel Aurora Kinase Inhibitor with Potent Antitumoral Activity. *Clin. Cancer Res.* **2006**, *12* (13), 4080–4089.
(26) Harrington, E. A.; Bebbington, D.; Moore, J.; Rasmussen, R. K.; Ajose-Adeogun, A. O.; Nakayama, T.; Graham, J. A.; Demur, C.; Hercend, T.; Diu-Hercend, A.; Su, M.; Golec, J. M. C.; Miller, K. M. VX-680, a Potent and Selective Small-Molecule Inhibitor of the Aurora Kinases, Suppresses Tumour Growth in Vivo. *Nat. Med.* **2004**, *10* (3), 262–267.
(27) Moriarty, K. J.; Koblish, H. K.; Garrabrant, T.; Maisuria, J.; Khalili, E.; Ali, F.; Petrounia, I. P.; Crysler, C. S.; Maroney, A. C.; Johnson, D. L., Jr. The Synthesis and SAR of 2-Amino-pyrrolo[2,3-*d*]pyrimidines: A New Class of Aurora-a Kinase Inhibitors. *Bioorg. Med. Chem. Lett.* **2006**, *16*, 5778–5783.
(28) Rawson, T. E.; Rüth, M.; Blackwood, E.; Burdick, D.; Corson, L.; Dotson, J.; Drummond, J.; Fields, C.; Georges, G. J.; Goller, B.; Halladay, J.; Hunsaker, T.; Kleinheinz, T.; Krell, H.-W.; Li, J.; Liang, J.; Limberg, A.; McNutt, A.; Moffat, J.; Phillips, G.; Ran, Y.; Safina, B.; Ultsch, M.; Walker, L.; Wiesmann, C.; Zhang, B.; Zhou, A.; Zhu, B.-Y.; Rüger, P.; Cochran, A. G. A Pentacyclic Aurora Kinase Inhibitor (AKI-001) with High in Vivo Potency and Oral Bioavailability. *J. Med. Chem.* **2008**, *51*, 4465–4475.

(29) Fancelli, D.; Moll, J.; Varasi, M.; Bravo, R.; Artico, R.; Berta, D.; Bindi, S.; Cameron, A.; Candiani, I.; Cappella, P.; Carpinelli, P.; Croci, W.; Forte, B.; Giorgini, M. L.; Klapwijk, J.; Marsiglio, A.; Pesenti, E.; Rocchetti, M.; Roletto, F.; Severino, D.; Soncini, C.; Storici, P.; Tonani, R.; Zugnoni, P.; Vianello, P. 1,4,5,6-Tetrahydropyrrolo[3,4-*c*]pyrazoles: Identification of a Potent Aurora Kinase Inhibitor with a Favourable Antitumour Kinase Inhibition Profile. *J. Med. Chem.* **2006**, *49* (24), 7247–7251.

(30) Carpinelli, P.; Ceruti, R.; Giorgini, M. L,; Cappella, P.; Gianellini, L.; Croci, V.; Degrassi, A.; Texido, G.; Rocchetti, M.; Vianello, P.; Rusconi, L.; Storici, P.; Zugnoni, P.; Arrigoni, C.; Soncini, C.; Alli, C.; Patton, V.; Marsiglio, A.; Ballinari, D.; Pesenti, E.; Fancelli, D.; Moll, J. PHA-739358, a Potent Inhibitor of Aurora Kinases with a Selective Target Inhibition Profile Relevant to Cancer. *Mol. Cancer Ther.* **2007**, *6* (12), 3158–3168.

(31) Oslob, J. D.; Romanowski, M. J.; Allen, D. A.; Baskaran, S.; Bui, M.; Elling, R. A.; Flanagan, W. M.; Fung, A. D.; Hanan, E. J.; Harris, S.; Heumann, S. A.; Hoch, U.; Jacobs, J. W.; Lam, J.; Lawrence, C. E.; McDowell, R. S.; Nannini, M. A.; Shen, W.; Silverman, J. A.; Sopko, M. M.; Tangonan, B. T.; Teague, J.; Yoburn, J. C.; Yu, C. H.; Zhong, M.; Zimmerman, C. M.; O'Brien, T.; Lew, W. Discovery of a Potent and Selective Aurora Kinase Inhibitor. *Bioorg. Med. Chem. Lett.* **2008**, *18*, 4880–4884.

(32) Mortlock, A. A.; Foote, K. M.; Heron, N. M.; Jung, F. H.; Pasquet, G.; Lohmann, J.-J. M.; Warin, N.; Renaud, F.; De Savi, C.; Roberts, N. J.; Johnson, T.; Dousson, C. B.; Hill, G. B.; Perkins, D.; Hatter, G.; Wilkinson, R. W.; Wedge, S. R.; Heaton, S. P.; Odedra, R.; Keen, N. J.; Crafter, C.; Brown, E.; Thompson, K.; Brightwell, S.; Khatri, L.; Brady, M. C.; Kearney, S.; McKillop, D.; Rhead, S.; Parry, T.; Green, S. Discovery, Synthesis and in Vivo Activity of a New Class of Pyrazoloquinazolines as Selective Inhibitors of Aurora B Kinase. *J. Med. Chem.* **2007**, *50*, 2213–2224.

(33) Wilkinson, R. W.; Odedra, R.; Heaton, S. P.; Wedge, S. R.; Keen, N. J.; Crafter, C.; Foster, J. R.; Brady, M. C.; Bigley, A.; Brown, E.; Byth, K. F.; Barrass, N. C.; Mundt, K. E.; Foote, K. M.; Heron, N. M.; Jung, F. H.; Mortlock, A. A.; Boyle, F. T.; Green, S. AZD1152, a Selective Inhibitor of Aurora B Kinase, Inhibits Human Tumour Xenograft Growth by Inducing Apoptosis. *Clin. Cancer Res.* **2007**, *13* (12), 3682–3688.

(34) Manfredi, M. G.; Ecsedy, J. A.; Meetze, K. A.; Balani, S. K.; Burenkova, O.; Chen, W.; Galvin, K. M.; Hoar, K. M.; Huck, J. J.; LeRoy, P. J.; Ray, E. T.; Sells, T. B.; Stringer, B.; Stroud, S. G.; Vos, T. J.; Weatherhead, G. S.; Wysong, D. R.; Zhang, M.; Bolen, J. B.; Claiborne, C. F. Antitumor Activity of MLN8054, an Orally Active Small-Molecule Inhibitor of Aurora A Kinase. *Proc. Natl. Acad. Sci. U.S.A.* **2007**, *104* (10), 4106–4111.

(35) The crystallographic data obtained from these soaking experiments were typically to a resolution of ~2.8 Å. While the gross resolution of these structures was modest, the electron density for the active site and ligands was clearly interpretable and ligand binding modes could routinely be assigned. Analysis of Aurora protein structures with **9**, **10**, and **16** bound showed clear electron density associated with the ligand. However, the continuity of the electron density was not maintained over the morpholine groups of the ligands because of their increased flexibility.

(36) In the primary cellular assay HCT116 cells were incubated with test compound for 72 h and then examined for signs of polyploidy. The numbers quoted refer to the lowest concentration of compound required to produce a distinct polyploid phenotyope (polyploidy is a direct result of Aurora B kinase inhibition). Key compounds **12** and **16** were also tested in a secondary cellular assay (HCT116 cell colony forming assay). In this case, IC_{50} numbers refer to the concentration of compounds required to inhibit colony formation by 50%. For reference purposes, compound **1** $IC_{50} = 24$ nM in the secondary assay.

(37) Misra, R. N.; Xiao, H.-Y.; Kim, K. S.; Lu, S.; Han, W.-C.; Barbosa, S. A.; Hunt, J. T.; Rawlins, D. B.; Shan, W.; Ahmed, S. Z.; Qian, L.; Chen, B.-C.; Zhao, R.; Bednarz, M. S.; Kellar, K. A.; Mulheron, J. G.; Batorsky, R.; Roongta, U.; Kamath, A.; Marathe, P.; Ranadive, S. A.; Sack, J. S.; Tokarski, J. S.; Pavletich, N. P.; Lee, F. Y. F.; Webster, K. R.; Kimball, S. D. *N*-(Cycloalkylamino)acyl-2-aminothiazole Inhibitors of Cyclin-Dependent Kinase 2. *N*-[5-[[[5-(1,1-Dimethylethyl)-2-oxazolyl]methyl]thio]-2-thiazolyl]-4- piperidinecarboxamide (BMS-387032), a Highly Efficacious and Selective Antitumor Agent. *J. Med. Chem.* **2004**, *47*, 1719–1728.

(38) Wenlock, M. C.; Austin, R. P.; Barton, P.; David, A. M.; Leeson, P. A Comparison of Physicochemical Property Profiles of Development and Marketed Oral Drugs. *J. Med. Chem.* **2003**, *46* (7), 1250–1256.

(39) Leeson, P. D.; Springthorpe, B. The Influence of Drug-like Concepts on Decision-Making in Medicinal Chemistry. *Nat. Rev. Drug Discovery* **2007**, *6* (11), 881–890.

(40) Lipinski, C. A.; Lombardo, F.; Dominy, B. W.; Feeny, P. J. Experimental and Computational Approaches To Estimate Solubility and Permeability in Drug Discovery and Development Settings. *Adv. Drug Delivery Rev.* **1997**, *23*, 3–25.

(41) Ravandi, F.; Foran, J.; Verstovsek, S.; Cortes, J.; Wierda, W.; Boone, P.; Borthakur, G.; Sweeney, T.; Kantarjian, H. A Phase I Trial of AT9283, a Multitargeted Kinase Inhibitor, in Patients with Refractory Hematological Malignancies. *Blood* **2007**, *110* (11), 904.

(42) Bayliss, R.; Sardon, T.; Vernos, I.; Conti, E. Structural Basis of Aurora-A Activation by TPX2 at the Mitotic Spindle. *Mol. Cell* **2003**, *12* (4), 851–862.

JM800984V